

NUMERICAL ANALYSIS OF SPECIFIC ABSORPTION RATE AND TO PROTECT HUMAN BRAIN FROM MICROWAVE RADIATION USING ELECTROMAGNETIC SHIELDING

Vakula Paranam S, Vasant Naidu

Dept of ECE, Sethu Institute of Technology, Pulloor, Kariapatti-626115, Tamil Nadu, India

ABSTRACT

The utilization of electromagnetic wave in various applications is increasing rapidly because of its advantages. Possibility of the electromagnetic wave impinges in a target, any one or combination of three interactions may occur: beam may be reflected, absorbed or may pass through the object. Only the absorbed fraction is harmful, it cause increase in temperature of human brain. Hence, to provide the shielding towards human brain from microwave radiation, the $TiEr_xHo_yFe_{2-x-y}$ material will be used $TiEr_xHo_yFe_{2-x-y}$ ferrite with $x=0.15, 0.7$ and $y=0.1, 0.06$ compositions were synthesized through the sol-gel method. These powders are calcined, compacted and sintered in a microwave furnace. The effect of Er substitution on phase composition, nanosize structure was analyzed by X-ray diffraction.. The nano material mixed with paint and it is coated on the glass surface to absorb the electromagnetic radiation. The depth of penetration and shielding effectiveness was measured. Shielding effectiveness increases upto 30 db as a function of frequency. The electrical, porosity studies and structural properties of $TiEr_xHo_yFe_{2-x-y}$ has been investigated and numerical analyzing of the reflection loss, dielectric properties for human brain in high frequency range has obtained. Moreover, the dielectric properties and temperature increase are proportional to the power of heating source. The specific absorption rate and the temperature distribution obtained by numerical solution of electromagnetic wave propagation to the human brain during exposure to mobile phone radiation are presented.

Keywords: specific absorption rate, Electrical Properties, Porosity, Shielding Effectiveness.

TABLE OF CONTENTS

| | |
|---|--|
| <p>I. INTRODUCTION.....2</p> <p>II.DOMAIN ENGINEERING.....2</p> <p style="padding-left: 20px;">A.Nano materials.....2</p> <p style="padding-left: 20px;">B.Applications of nano ferrites.....2</p> <p style="padding-left: 20px;">C.History of lanthanides doping.....3</p> <p style="padding-left: 20px;">D.Preparation of nano ferrite.....3</p> <p style="padding-left: 20px;">E.History of meta materials.....3</p> <p style="padding-left: 20px;">F.Scope of Work.....3</p> <p>III.PHYSICAL BASIS OF THE DOMAIN ENGINEERING.....3</p> <p style="padding-left: 20px;">A.Existing problem of micro and nano domain engineering.....3</p> <p style="padding-left: 20px;">B.Main stages of nano meta material development.....3</p> <p>IV.PHYSICAL BASIS AND NUMERICAL DESCRIPTION.....4</p> | <p style="padding-left: 20px;">A.Methods and model.....4</p> <p style="padding-left: 20px;">B.Physical Model.....4</p> <p>V.PREPARATION OF NANO FERRITE COMPOSITES.....5</p> <p style="padding-left: 20px;">A.Nano powder for micro-nano domain engineering5</p> <p>VI.CRYSTAL STRUCTURE OF HOLMIUM AND ERBIUM TITANIUM FERRITE FAMILY.....5</p> <p>VII.CHARACTERIZATION ANALYSIS.....5</p> <p style="padding-left: 20px;">A.Electrical Properties.....5</p> <p style="padding-left: 20px;">B.X-Ray Diffraction.....6</p> <p>VII.ANALYSIS METHOD.....6</p> <p>IX.RESULTS AND DISCUSSIONS.....6</p> <p style="padding-left: 20px;">A.Electrical properties.....6</p> <p style="padding-left: 20px;">B.Semi conductivity test.....7</p> <p style="padding-left: 20px;">C.XRD results.....8</p> <p style="padding-left: 20px;">D.Shielding effectiveness.....8</p> <p>X.CONCLUSION.....11</p> |
|---|--|

I. INTRODUCTION

In recent years, there is an increasing public concern about the health implications of the use of mobile phone, as a result of the rapid growth in the use of mobile phone throughout the world. Although the safety standards are regulated in terms of the peak specific absorption rate (SAR) value of tissue, the maximum temperature increase in the human head caused by electromagnetic energy absorption is an actual influence of the dominant factors which induce adverse physiological effects [1]. The severity of the physiological effect produced by small temperature increases can be expected to worsen in sensitive organs. Hence to protect the human brain from microwave radiation nano materials are used. These nano materials help to shield the radiations from microwave devices [2].

Nanoscale materials have attracted much attention recently due to many unusual properties predicted. As commercial, military, and scientific electronic devices and communication instruments are used more and more widely, electromagnetic interference (EMI) shielding of radio frequency radiation continues to be a more serious concern in this modern society [3].

Light weight EMI shielding is needed to protect the workspace and environment from radiation coming from computers and telecommunication equipment as well as for protection for sensitive circuits [4].

Compared to conventional metal-based EMI shielding materials, nano composites have gained popularity in recent years. The EMI shielding efficiency (SE) of a composite material depends on many factors, including the dielectric constant, and aspect ratio [5]. The high conductivity, small diameter, high aspect ratio, and super mechanical strength and so on of nano materials make them an excellent option to create conductive composites for high-performance EMI shielding materials at low filling concentration.

II. DOMAIN ENGINEERING

Electromagnetic interference shielding refers to the reflection and / or adsorption of electromagnetic radiation by a material, which thereby acts as a shield against the penetration of the radiation through the shield. There are three mechanisms for providing Electromagnetic interference shielding. They are absorption, reflection

and multiple reflections. Various types of shielding materials are used recently [6].

Due to their light weight, versatility and processability, nano materials had been used in enclosures for electronic and electrical devices to satisfy electromagnetic shielding requirements.

A device is considered electromagnetically shielded with its surrounding if it does not interfere with other devices or itself, and it does not affected by emissions from other devices [7]. Therefore, a good shielding material should prevent both incoming and outgoing electromagnetic interference (EMI). EMI shielding effectiveness (SE) is expressed in decibel (dB). A shielding effectiveness of 30 dB, corresponding to 99.9% attenuation of the EMI radiation, is considered an adequate level of shielding for many applications

A. Nano Materials

On account of the excellent electric and magnetic properties, Ferrite materials are being served as electromagnetic interference suppressors, dielectric counterparts etc. Due to the localized nature of 4f electrons Rare earth (R) elements have the properties of large magnetic moments, large magneto crystalline anisotropy and very large magnetostriction at low temperatures. Structural distortion is caused by substituting very small amount of rare earth cations in Co-Ti ferrites lattice, So that the magnetic properties of as prepared materials are enhanced [8].

In microwave absorbing materials the spinel Titanium ferrite plays an important role in the frequencies ranges from a few hundred hertz to several Megahertz. It is due to the properties of high saturation magnetization, high coercivity, strong anisotropy along with good mechanical hardness and chemical stability. It also has high permeability and high electrical resistivity in this frequency range [9].

B. Application of Nano Ferrites

The applications like information storage systems, magnetic cores, and medical diagnostics use Spinel ferrites for their useful electrical and magnetic properties. Many researches reveal that Nano ferrite material is used in applications like audio frequency and high frequency transformers coil's core, optical displays, electromagnetic wave absorption, microwave absorbers, wave guides in the GHz region, optical devices etc [10]. Co- Ti ferrites is

most popular in switching and memory device applications.

C. History of lanthanide doping.

The usual magnetic, optical and electrical properties of rare earth doped ferrites had attracted the attention of many researches in recent years, by using energy transfer between co-doping of two or more types of lanthanides within the same host material. The most efficient energy transfer processes involve resonant overlap between the emission band of the donor ion and the absorption band of the acceptor ion [11,12]. Using the Dieke diagram, the study of relative positioning amongst the lanthanide energy levels is being made to obtain an excellent opportunity for preparing a material, by using the advantages of resonant energy transfer [13].

Lanthanide has become main contributor, to change the various ferrite properties and thus improved dc resistivity, negative permittivity and low relative loss factor [14]. It was observed that, certain lanthanide, such as Ho, Pr, Gd, Dy, Sm and sometimes Er, can improve the resistance of the magnesium ferrite. Here the substitution of the small amount of rare earth ions may bring important changes in electrical, structural and magnetic properties of as prepared ferrite material [15].

Partially filled of 4f inner shells are responsible for the characteristics of optical magnetic properties of lanthanides as very well clearly in dieke diagram [16]. Judd and Oflet (1962) investigated parity states on the inter configurational transition probabilities and the selection rule of lanthanides ions [17,18].

D. Preparation of nano ferrite

Preparing nano ferrite by sol-gel route has the significant advantage such as good stoichiometric control and to produce the ultra-fine (nano) particles with narrow size distribution in relatively short processing time at room temperature [19].

E. History of meta materials

Meta materials are artificial materials engineered to have properties that may not be found in nature. The meta materials in electromagnetic, acoustic and seismic meta field plays a dominant role. Thus the meta material becomes a potential candidate for active research [20]. Therefore the meta materials has found place in remote aerospace applications, sensors, infrastructure monitoring and even shielding

the structures from seismic waves during earth quakes.

F. Scope of Work

The goal of the work is to synthesize the nano sized Er-Ho substituted titanium ferrite by using sol-gel auto combustion method and to exhibit structural properties of the material. The investigation of electromagnetic absorption properties of nano composite materials are measured theoretically and experimentally. The shielding effectiveness as a function of frequency is determined and also numerical analysis of temperature increase in human brain is obtained.

III. PHYSICAL BASIS OF THE DOMAIN ENGINEERING

A. Existing problem of micro and nano domain engineering

It is necessary to overcome the several barriers in the synthesization of nano powders from the composites of lanthanides doubly doped with magnesium ferrite.

The most important problem is the magnesium ferrite is in non stoichiometry state (i.e) magnesium ferrite has the leakage current arising out of stoichiometry. This condition arises mostly because of the complexity in obtaining stoichiometric single phase magnesium ferrite materials.

B. Main stages of nano meta material development

The nano meta material development consists of three main stages: (1) material selection (2) synthesis of nano meta material (3) Characterization of materials.

“Material Selection” is the most important and difficult stage for the direct experimental. Already, TiO_2 is in non stoichiometry. Effort to enhance the electrical and magnetic properties had been done by using the rare earth elements such as Holmium (Ho), Erbium (Er), Samarium (Sm) and Cerium (Ce) etc. Here, the lanthanides Holmium and Erbium are chosen and it's doubly doped with Titanium ferrite.

“Synthesis of nano meta material” the methods for nano materials synthesization are grouped into two categories, “top-down” and “bottom-up” approach. The first involves the division of a massive solid into smaller and smaller portions, successively reaching to nanometre size. The second, “bottom-up”, method of nanoparticle fabrication involves the condensation of

atoms or molecular entities in a gas phase or in solution to form the material in the nanometer range.

There are many bottom up methods of synthesizing metal oxide nanomaterials, such as hydrothermal, combustion synthesis, gas-phase methods, microwave synthesis and sol-gel processing. Here, Sol – gel technique is used for synthesization of nano materials.

“Characterization of materials” includes the XRD and VSM studies. XRD had been done by using PAN analytical X’per PRO, to study the lattice constant of nano material. VSM had been used to study about magnetic properties of the material.

IV. PHYSICAL BASIS AND NUMERICAL DESCRIPTION

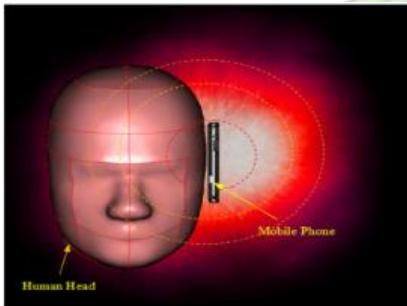


Fig 1 Human head exposed to mobile phone radiation

Fig. 1 shows the radiation of electromagnetic energy from mobile phone to a realistic human head model. Due to ethical consideration, exposing a human to electromagnetic fields for experimental purposes is limited. An analysis of dielectric and thermal properties for the human head exposed to mobile phone radiation is illustrated.

A. Methods and model

The first step in evaluating the effects of a certain exposure to radiation in the human head is the determination of the induced internal electromagnetic field and its spatial distribution. Thereafter, electromagnetic energy absorption which results in temperature increases within the human head and other interactions can be considered.

B. Physical Model.

In this study, a patch antenna of a mobile phone located at the left side of a human head with a certain position is considered as a near-field radiation source for human head models.

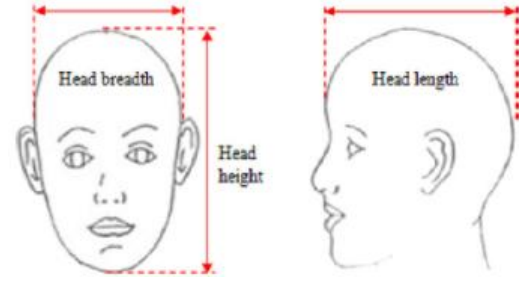


Fig 2 Head dimensions

Table 1 Head dimensions used in this study

| Head parameters | Adult | 7 year old child |
|-----------------|-------|------------------|
| Head breadth | 16 | 14.9 |
| Head length | 18.8 | 17.3 |
| Head height | 23.7 | 20.8 |

Table 2 Dielectric properties of tissue at 900MHz

| Parameter | Adult | | 7 year old child | |
|-----------|--------------|----------|------------------|----------|
| | ϵ_r | σ | ϵ_r | Σ |
| Brain | 45.805 | 0.765 | 46.75 | 0.78 |

Table 3 Thermal properties of tissue

| Type of tissue | ρ | K | C | Q_{met} | w_b |
|----------------|--------|-------|------|-----------|-----------------------|
| Brain | 1038 | 0.535 | 3650 | 7100 | 8.83×10^{-3} |

Figure 2 and Table 1 give adult and child head dimensions used in this study, which are directly taken from statistical body-size data. The dielectric properties of tissues at the frequency of 900 MHz and thermal properties are given in Tables 2 and 3 respectively.

Hence, to protect the human head from radiation EMI shielding is required. EMI shielding is done using these processes. Sample preparation includes material selection, calculation, measurement, doping, stirring, pelletisation and sintering. The process is performed by using Sol – Gel technique.

V. PREPARATION OF NANO FERRITE COMPOSITES

A. Nano powder for micro-nano domain engineering

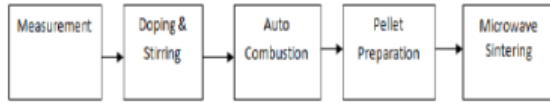


Fig 3 SOL-GEL process

The nano ferrite materials [16-17] have been prepared through sol-gel method. Analytical grade Titanium Oxide [TiO₂], Holmium Nitrate [Ho(NO₃)₂], Erbium Nitrate [Er(NO₃)₂], Ferrite nitrate Fe(NO₃)₂, Citric acid [C₆H₈O₇] the above materials had been used to prepare the TiEr_xHo_yFe_{2-x-y}O₄ ferrite with various compositions x=0.15,0.7 and y=0.1,0.06 respectively. Christo Ananth et al. [17] discussed about an eye blinking sensor. Nowadays heart attack patients are increasing day by day."Though it is tough to save the heart attack patients, we can increase the statistics of saving the life of patients & the life of others whom they are responsible for. The main design of this project is to track the heart attack of patients who are suffering from any attacks during driving and send them a medical need & thereby to stop the vehicle to ensure that the persons along them are safe from accident. Here, an eye blinking sensor is used to sense the blinking of the eye. spO₂ sensor checks the pulse rate of the patient. Both are connected to micro controller.If eye blinking gets stopped then the signal is sent to the controller to make an alarm through the buffer. If spO₂ sensor senses a variation in pulse or low oxygen content in blood, it may results in heart failure and therefore the controller stops the motor of the vehicle. Then Tarang F4 transmitter is used to send the vehicle number & the mobile number of the patient to a nearest medical station within 25 km for medical aid. The pulse rate monitored via LCD .The Tarang F4 receiver receives the signal and passes through controller and the number gets displayed in the LCD screen and an alarm is produced through a buzzer as soon the signal is received.

VI. CRYSTAL STRUCTURE OF HOLMIUM AND ERBIUM TITANIUM FERRITE FAMILY

Crystal structure of the as prepared TiEr_xHo_yFe_{2-x-y}O₄ powder was obtained using crystal maker 9.2.3.After feeding the various data's such as radius, lattice parameter etc., about the elements present in the nano powder. The crystal structure was obtained as shown in figure 4.

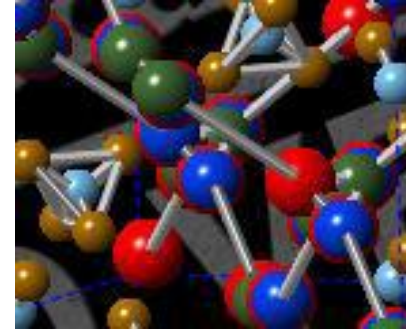


Fig 4 Bonding structure of TiEr_xHo_yFe_{2-x-y}O₄

It has been found that the spacegroup for the crystal has been mentioned as Fd3̄m cubic.Further density, porosity and bonding distance between the elements were also obtained. These values matched with the experimental values

Table 4bond length for MgGd_xPr_yFe_{2-x-y}O₄

| Material | Bond Length | | | |
|--|---------------------|---------------------|---------|---------|
| | Fe – O ₄ | Ti – O ₄ | Fe – Er | Fe – Ho |
| TiEr _x Ho _y Fe _{2-x-y} O ₄ | 1.3995 | 1.275 | 2.5969 | 3.314 |

Densities of the chemical elements to

| Material | Material properties | | | |
|--|------------------------------|-------------------------|--------------|------------|
| | Density (Kg/m ²) | Atomic Density (Atom/Å) | Porosity (Å) | |
| | | | Filled Space | Void Space |
| TiEr _x Ho _y Fe _{2-x-y} O ₄ | 43,177.1563 | 0.2656 | 118.779 | 438.735 |

increase uniformly with atomic weight, but this is not what happens; density depends on the volume as well as the mass, and the volume occupied by a given mass of an element, and these volumes can vary in a non-uniform way for two reasons:

The sizes (atomic radii) follow the zig-zag progression that characterizes the other periodic properties of the elements, with atomic volumes diminishing with increasing nuclear charge across each period. Porosity or void fraction is a measure of the empty space in that material.

Table 5 Material Properties

VII. CHARACTERIZATION ANALYSIS

A. ELECTRICAL PROPERTIES

N4L LCR meter has been studied for the permittivity measurements. The experimental setup for measured the dielectric properties in the microwave region at the frequency range varies from 1 KHz to 35 MHz. The microwave properties of the

samples Gd (x) - Pr (y) doped magnesium ferrite had been investigated.

The dielectric constant (ϵ_r) was calculated from the relation:

$$\epsilon_r = \frac{CL}{\epsilon_0 A}$$

Where, C(F) are the capacitance of the material, L(cm) is the thickness of the samples, ϵ_0 (F/cm) is the free space permittivity, A(cm²) is the area of the samples.

B. X-RAY DIFFRACTION

The erbium-substituted titanium ferrite samples were characterized by using X-ray powder diffraction study which is used for structural analysis. The lattice parameter “a” for all the samples has been calculated for prominent peak using Bragg’s Equation:

$$a = d_{hkl} \sqrt{(h^2 + k^2 + l^2)}$$

In Hall-Williamson method it is assumed that the line-broadening of a Bragg reflection originating from the small crystallite size follows Scherrer equation:

$$\beta = \frac{k\lambda}{D \cos \theta}$$

where λ is the X-ray wavelength, K is the Scherrer constant ($k \approx 1$), θ is the Bragg angle, and D is the average crystallite size.

By plotting the value of $\beta \cos \theta$, the crystallite size and lattice strain are estimated. The slope of the line gives the lattice strain ϵ and the crystallite size D can be evaluated from the intercept of this line on the y-axis:

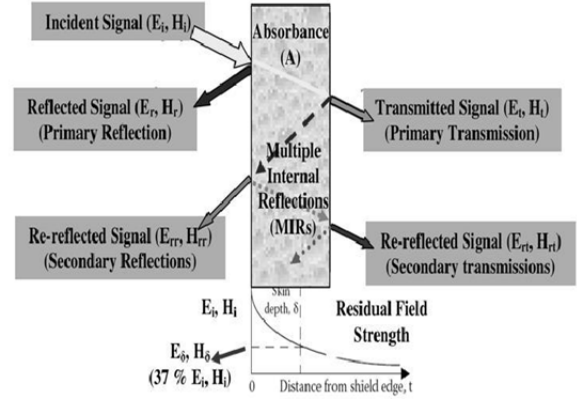
$$D = \lambda / \text{intercept}$$

VIII. ANALYSIS METHOD

Schelkunoff model describes the shielding mechanism of material against electromagnetic radiation [13]. The schematic representation of the model is shown in the figure 5.

The well known properties related to the shielding material are δ the skin depth, σ the conductivity and μ the permeability, and is defined in equation,

$$\delta = \sqrt{\frac{1}{\pi f \mu \sigma}}$$



The skin depth is dependent on frequency f: as the The table 3 and 4 shows that the ϵ values, it is also seen that the value of ϵ increases with the addition of erbium and holmium atom concentration, while the capacitance value remains fairly constant over the frequency range of study. If frequency increases the skin depth decreases, and so the thickness of a material required to effectively shield is reduced.

The measure of shielding effectiveness (SE) is used to describe how well any given material attenuates an electromagnetic wave. The accepted

Fig 5 Mechanism of electromagnetic shielding

method of measuring this effect is to simply measure the electric field strength on either side of the material in question. The field strength on the illuminated (left hand) side of Medium 2 will be higher than that on the shadowed side (i.e E_i > E_t); and a simple and accepted way of expressing this is to take a ratio between these two quantities.

The SE can be given in the form of the electric field strength E, the magnetic field strength H or the power density S. Usually, the SE is expressed in decibels, obtaining the following forms,

| Capacitance | Thickness | Area | Permittivity |
|-------------|-----------|-------|--------------|
| 77.609 | 0.198 | 1.216 | 148.3351 |
| 55.913 | 0.198 | 1.216 | 110.6864 |
| 44.407 | 0.198 | 1.216 | 84.873 |

$$SE_{dB} = 20 \log \left(\frac{E_i}{E_t} \right)$$

where the denominators E_i is the unshielded reference measurements, equivalent to the incident

wave E_i in figure 1, and the numerator E_t is the shielded measurements, equivalent to the transmitted wave E_t . The process of obtaining the two quantities used to obtain the SE is widely used in both material shielding and enclosure experiments and tests.

IX. RESULTS AND DISCUSSIONS

A. Electrical Properties

Table 6 capacitance and permittivity for TiErHoFe

The Permittivity is calculated for $x=0.15$ & $y=0.1$ and listed in the table 3. It is also seen that the value of capacitance increases with the addition of Erbium and Holmium atom concentration. The change of permittivity which depends on the Erbium & Holmium concentration is shown in table 6.

Table 7 dielectric constant for TiErHoFe

| X proportion | Y proportion | Dielectric constant |
|--------------|--------------|---------------------|
| 0.15 | 0.1 | 58.6341 |
| 0.7 | 0.06 | 65.2513 |

Hence, the corrected porosity is determined by,

$$\epsilon_m = \epsilon \left[1 - \frac{3p(\epsilon - 1)}{2\epsilon + 1} \right]$$

By increasing the X and Y concentration, porosity value and permittivity for TiErHoFe gets increased.

Table 8 corrected permittivity value from porosity

| Porosity | Density | Corrected permittivity |
|----------|---------|------------------------|
| 0.4348 | 3.176 | 3.699 |

i) Porosity Studies

Porosity or void fraction is a measure of the void (i.e., "empty") spaces in a material, and is a fraction of the volume of voids over the total volume, between 0 and 1, or as a percentage between 0 and 100%

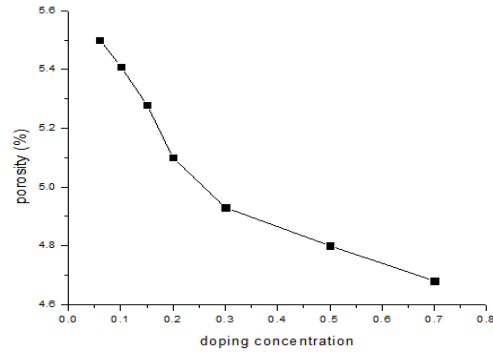
The bulk density was calculated by the following equation

$$dB = \frac{m}{V}$$

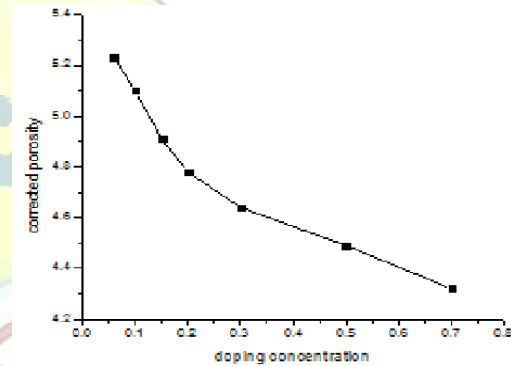
Here m is the mass of the pellet and V is the volume of the pellet. Later by substituting for d_B and d_X X-ray density in Eq. the information regarding the porosity of the samples were obtained. The porosity behavior of the materials with respect to the doping concentration is shown in figure.

$$\rho = \frac{dB}{dX}$$

It is also seen that the density of titanium ferrite increased with the doping concentration of Er and Ho shown in Fig, it is because the molecular weight of



the holmium (164.93 amu) and erbium (167.26 amu) are higher than the molecular weight of Fe (55.845 amu), since the Er and Ho atoms are replacing the Fe



atoms causes the increase in density, and decrease in the porosity. Here the percentage of porosity of each sample was calculated using Eq. It was found that the percentage of porosity in Er-Ho doped magnesium ferrite decreased from 5.5 to 4.7 with respect to the increasing doping concentration as shown in Fig 6,

B. Semi Conductivity Test

Four probe measurements was performed to check the semiconductor property of the material. Four probe measurements include the microwave oven, low current source, PID controller. The pellet with silver coating was used here. If the voltage decreases with the increase in temperature, then it is n-type material. If voltage increases, it is p-type material. Here as prepared sample is n-type material.

C. XRD Results

The size of the nano particle was determined using X-ray diffraction (XRD) characterization method. These XRD was in according to JCPDS card

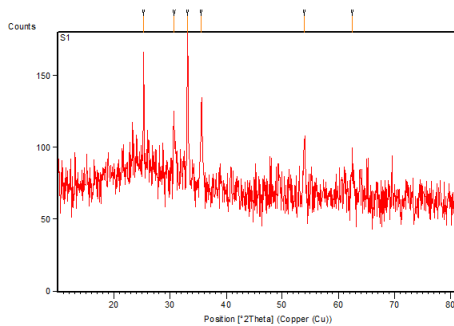
Number for erbium: 70-953. The shape of the peak, particularly its width, contains the useful information about the grain size of the corresponding crystalline phase. Therefore the width of the peak, one can obtain the value of the main grain size D using the Debye – Sheerer equation.

$$D = \frac{0.94\lambda}{\beta \cos\theta}$$

The samples are formed in single spinel phase. Where λ is the X-ray wavelength ($\lambda=1.54 \text{ \AA}$) and β width of the diffraction peak at HM for the diffraction angle 2θ . TiFe_2O_4 doped Er-Ho shows that present of single phase cubic spinel structure shown in fig 4.

Fig9 XRD graph of Er-Ho doped Titanium Ferrite for x=0.15, y=0.1

Fig 10 XRD graph of Er-Ho doped Titanium Ferrite for x=0.7, y=0.06



The lattice constant and particle size of the material MGPF using XRD analysis is listed in the

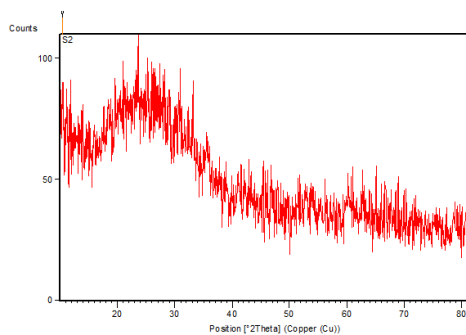


table 1. The lattice parameter obtained from the XRD diffraction peaks were 8.305 and 8.448 \AA . It is seen that the lattice parameter increases linearly with the increase of Ho^{3+} and Er^{3+} ions. This confirms the increase in lattice parameter is due to the larger ionic radius of Ho^{3+} (1.04 \AA) and Er^{3+} (1.03 \AA) than those

of host cation i.e., TiO_2 (0.75 \AA) and Fe^{3+} (0.69 \AA).

Table 9 Particle Size and Lattice Constant from XRD Studies

As prepared TiErHoFe a noticeable peak appears at $2\theta=45^\circ$ with an average particle size of about 50.8 nm randomly distributed in an amorphous

| Material - TiErHoFe | Particle Size (nm) | Lattice Constant |
|------------------------------|--------------------|------------------|
| X=0.15, Y=0.1 | 28.11 | 8.305 |
| X=0.7, Y=0.06 | 53.27 | 8.448 |

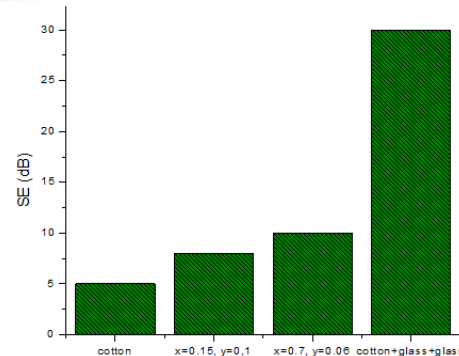
matrix the diffraction spectra must be attributed to the superposition of those peaks corresponding to the crystalline and amorphous phases.

Analysis of the X-Ray diffraction performed at the room temperature reveals that the structure of all the as-prepared samples consists of cubic $\text{Fd}3m$. The peaks shown in XRD pattern are indexed to a mixture of different compounds and other remaining minor peaks attributed as impurity.

E. Shielding Effectiveness

The Electromagnetic shielding effectiveness (SE) is measured in X-band (8-12 GHz) frequency range. SE has been investigated using combination of cotton with TiErHoFe having varying concentration such as x=0.15, y=0.1, and x=0.7, y=0.06. This sample presents an average electromagnetic shielding effectiveness of about 30 dB with the best efficiency for protection against electromagnetic radiation in the 8-12 GHz frequency range. Because, cotton is the best radiation barrier in nature. Hence the SE is considerably increased

This sample exhibits electromagnetic shielding effectiveness of about 30 dB with the best efficiency for protection against electromagnetic radiation in the



X-band It is shown that shielding effectiveness increases as the frequency increases. Moreover, the

shielding effectiveness is increased as the thickness of the material increases.

By using this TiErHoFe material, the human brain has been protected from microwave radiations. The temperature and heat transfer of the human brain are considerably controlled. The conditions of human brain in exposure field at various cases are shown below.

a) Correlation of grasshopper brain with human brain:

The experiment was performed on one grasshopper placed in polythene transparent bag of 10 micron thick, for exposure with small opening on the top and small pin holes pierced in the bag providing enough air. Here function generator combined with microstrip antenna having operating frequency as 1.5GHz is used as microwave source.



Fig 10 Insect exposure in microwave radiation

As the experiment is conducted for low power level so it is best suited for this experiment. Experiment was started at 11:00AM and lasted till 12:15 AM at power of 6.132 W at temperature of 29°C.

- a) **At 11:00 AM:** On striking the polythene by fingers, it respond quickly, showing it is active. .
- b) **At 11:30AM:** There is some sort of laziness and dullness in their behavior but still sometimes it show opposition.\
- c) **At 12:00 PM:** It is trying to move away from the vicinity of EM exposure.
- d) **At 12:05 PM** There was no movement found during this time as if they are unconscious.
- e) Effect of radiation is more is younger insect than the elder one. The insects was the most susceptible to microwave energy and adults were the least susceptible. There was a significant decrease in the movement with an increase exposure time. Capacity of speed of their movement was decreased with an increase in exposure time. This grasshopper's

experiment is taken as the reference for human brain numerical analysis.

i) The condition for EM Field penetrate in human brain,

$$\frac{1}{\mu_r} * E - K_o^2 \epsilon_r * E = 0$$

Electric field intensity is varied frequency and distance as,

$$E = 106.92 + ERP(dB/K) - 20 \log(Km)$$

Table 10 Electric field intensity for distance of 1cm and 2cm

| Frequency | Distance | Electric field intensity |
|-----------|----------|--------------------------|
| 900 | 1 | 14.792 |
| 1800 | 2 | 20.189 |

ii) Interaction of Electromagnetic Waves and Human Tissue

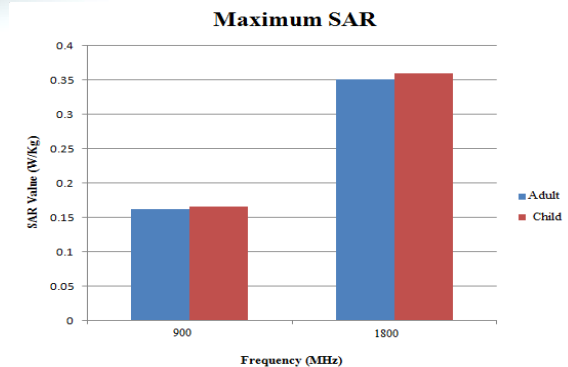
Interaction of electromagnetic fields and biological tissue can be defined in terms of SAR. When electromagnetic waves propagate through the human tissue, the energy of electromagnetic wave propagation is absorbed by the tissue. The specific absorption rate is defined as power dissipation rate normalized by material density. The specific absorption rate is given by

$$SAR = \frac{\sigma}{\rho} |E|^2$$

The value for the electrical conductivity and magnetic permeability of adults and child are taken from the table 2 and 3

Fig 11 SAR value for corresponding frequency

The maximum electric field intensity in outer parts of the adult head displays a little higher



value than that of the child head due to larger area of adult head exposed to the electric field. However, the

electric field can penetrate deeper into the child head because of its small size, which results in a high specific absorption rate in tissues deep inside the child head.

The human head is depended on the effect of the dielectric properties of human tissue. With penetration into the head, the SAR values decrease rapidly along the distance. However, it can be observed that there is a deeper penetration of mobile phone radiation into the child head. Comparing these results to the ICNIRP limit of SAR value (2W/kg), one sees that the resulting SAR from this study does not exceed the limit value in all cases.

ii) Equations for Heat Transfer Analysis:

To solve the thermal problem, the temperature distribution in the human head has been evaluated by the bioheat equation according to Maxwell's equations. The temperature distribution corresponds to the SAR. This is because the SAR within the human head distributes, owing to energy absorption. Thereafter, the absorbed energy is converted to thermal energy, which increases the tissue temperature.

The temperature distribution within the human head is obtained by solving Pennes' bioheat equation. The transient bioheat equation describes effectively how heat transfer occurs within the human head, and the equation can be written as,

$$\rho c \frac{dT}{dt} = \nabla \cdot (k \nabla T) + \rho_b c_b w_b (T_b - T) + Q_{met} + Q_{ext}$$

Biological properties of the brain tissue:

k : thermal conductivity of the brain tissue ($W m^{-1} \text{ } ^\circ C^{-1}$) = 0.45–0.6,

ρ_b : density of the brain tissue ($kg m^{-3}$) = 1040,

C_p : specific heat of the brain tissue ($J kg^{-1} \text{ } ^\circ C^{-1}$) = 3650,

σ : electrical conductivity ($S m^{-1}$) = 0.15–0.35,

T_i : initial temperature of the brain tissue = 37 $^\circ C$.

Biological properties of the blood:

ω_b : volumetric blood perfusion rate per unit volume ($ml s^{-1} cm^{-3}$) = 0.004–0.012,

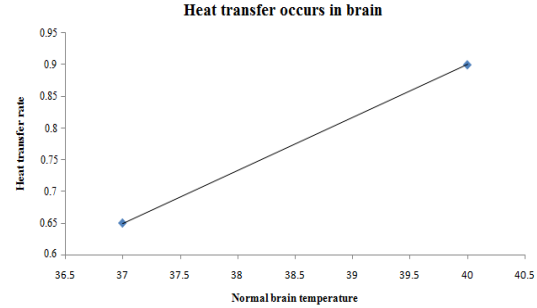
ρ_b : density of the blood ($kg m^{-3}$) = 1057,

C_b : specific heat of the blood ($J kg^{-1} \text{ } ^\circ C^{-1}$) = 3600,

T_b : body core temperature = 36.7 $^\circ C$.

Fig 12 Heat transfer occurs in brain

In addition, it is found that the temperature distributions are not directly proportional to the local



SAR values. Nevertheless, these are also related to parameters, such as thermal conductivity, dielectric properties, blood perfusion rate, etc.

It is therefore important to use a strongly coupled model for thermal and electromagnetic wave propagation to assess the health effects of exposure to electromagnetic waves. Heat transfer present in brain probably increases the temperature of human brain. SAR and heat transfer is directly proportional to metabolic activity and blood perfusion rate.

Moreover, it is found that the temperature distributions in human head induced by mobile phone radiation are not directly related to the SAR distribution, due to the effects of dielectric properties, thermal properties, blood perfusion, and penetration depth of the electromagnetic power.

If the human is exposed to high radiation, the metabolic rate and blood perfusion rate is highly affected. Hence these factors are considered.

There are two cases where the temperature increases in two increasingly detailed situations.

Case 1: Temperature distribution in human brain without perfusion rate and metabolic activity.

By using, Pennes bio-heat equation

Fig 12 Temperature increases without perfusion rate and metabolic activity

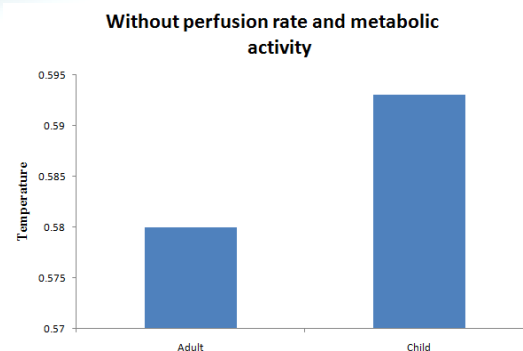
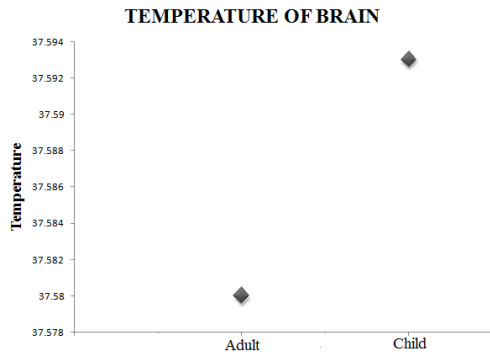


Fig 13 Temperature of brain without perfusion and metabolic rate



The brain has a high metabolic heat generation rate and consequently a higher temperature than tissues with a lower rate of metabolic heat generation. Hence, without considering the perfusion rate and metabolic activity, the temperature will automatically increase.

Case 2: Temperature distribution in human brain with perfusion rate and without metabolic activity
Fig 14 Temperature increases with perfusion rate and without metabolic rate

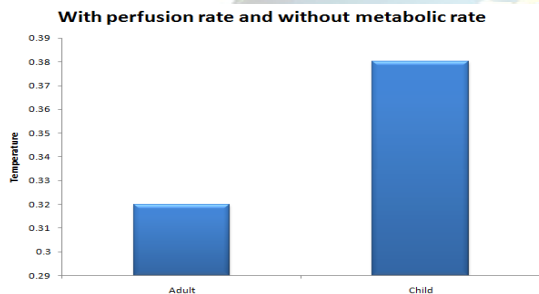
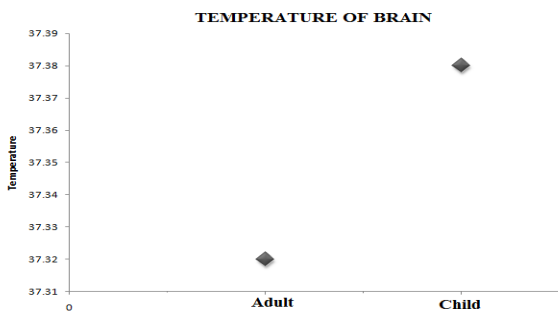


Fig 15 Temperature of brain with perfusion and without metabolic rate



The temperature of brain is increasing in two cases. Hence to protect the human brain from increase in temperature the material $TiEr_xHo_yFe_{2-x-y}$ is preferred. By using this material SAR rate and temperature of brain is decreased.

X. CONCLUSION

The numerical simulation of SAR and temperature distributions in adult and child heads exposed to mobile phone radiation at the frequency of 900 MHz with the radiated power of 1.0W was analyzed. The numerical simulations in this study show several important features of the specific absorption rate and temperature in the human head. The result shows that, the maximum temperature increase in brain of child is greater than the temperature increase in adult and also SAR value of child's brain is higher than the SAR value of adult's brain. To protect children from radiation, the TiErHoFe shielding material is prepared. Doubly doped Titanium Ferrite nano ferrites structures have been successfully synthesized through sol gel auto combustion method. The structural analysis was done by using X-ray Diffraction study. Dielectric properties were studied by using LCR Meter. For the improvement in the shielding, the material is mixed with paint to enhance the shielding effectiveness. The nano ferrite showed higher EM absorption and shielding effectiveness due to the larger magnetic anisotropy of Ti ferrite nano particles. Hence by using TiErHoFe temperature of human brain is considerably decreased.

REFERENCES

- [1] H. Andriamiharinjaka, F. Razafimahery and L. R. Rakotomanana, Effect of wave propagation and heat transfer in Skull-csf-brain system exposed to electromagnetic Wave, International Conference on Computational Bioengineering ICCB (2015).
- [2] Teerapot Wessapan, Phadungsak Rattanadecho, Numerical Analysis of Specific Absorption Rate and Heat Transfer in Human Head Subjected to Mobile Phone Radiation: Effects of User Age and Radiated Power, journal of heat transfer · december (2012) Vol. 134 / 121101-1.
- [3] Nicolai et.al "Ferromagnetic materials" Pub Wohlfarth Amsterdam: North-Holland pp-243, (1985).
- [4] Rao Arsalan Khushnood, Sajjad Ahmad, Patrizia Savi, Jean-Marc Tulliani, Mauro Giorcelli, Giuseppe Andrea Ferro, Improvement in electromagnetic interference shielding effectiveness of cement composites using carbonaceous nano/micro inerts,

- Construction and Building Materials, (2015) 208–216.
- [5] Fei-Shuo Hung, Fei-Yi Hung, Che-Ming Chiang and Truan-Sheng Lui, Electromagnetic Interference Shielding Characteristics of Sn-Al Powder Coating Layers, Materials Transactions, Vol. 49, No. 3 (2008) pp. 655 to 660.
- [6] Davide Micheli n, CarmeloApollo, RobertoPastore, Ramon Bueno Morles, Susanna Laurenzi, Mario Marchetti, Nano structured composite materials for electromagnetic interference shielding applications, Acta Astronautica 69(2011)747–757.
- [7] GUO Shuxia, DONG Zhongyao, HU Zhantao, HU Chufeng, Simulation of Dynamic Electromagnetic Interference Environment for Unmanned Aerial Vehicle Data Link, China Communications, July 2013.
- [8] E.Melagiriappa .et al “Dielectric behavior and AC Electrical conductivity study of Sm³⁺ substituted Mg-Zn ferrite” material chemistry and physics , 8-73, (2000).
- [9] Vasant Naidu, S.K.A.Ahamed Kandu Sahib, M.Suganthi, Chandra Prakash, Study of Electrical and Magnetic properties in Nano sized Ce-Gd Doped Magnesium Ferrite, International Journal of Computer Applications, 27[5], (2011) 40-45.
- [10] B.Malkin. Spectroscopic properties of rare earths in optical materials, Springer-Verlag, Berlin, 130- 190, (2005),
- [11] D.Andrews, A unified theory of radiative and radiation less molecular energy transfer, chem.. phys. 135, 195 (1989).
- [12] F.Auzel, “upconversion and anti-stokes processes with f and d ions in solids”, chem.. Rev. 104, 139 (2004).
- [13] G. Dieke, Spectra and energy levels of Rare Earth ions in crystal, Inter science Publishers NewYork, 1968.
- [14] B.Henderson and G.Imbusch, “optical spectroscopy of inorganic solids”, clarendon press, oxford, (1989).
- [15] G.Blasse and B.Grabmaier, luminescent materials, Springer-Verlag, Berlin, Germany, (1994).
- [16] X Liu., W Zhong., S Yang., Z Yu., B Gu., and Y Du., Influence of La³⁺ substitution on the structural and magnetic properties of M-type strontium ferrites, J. Magn. Magn. Mater., 238 (2-3): 207(2002).
- [17] Christo Ananth, S.Shafiqa Shalaysha, M.Vaishnavi, J.Sasi Rabiyyathul Sabena, A.P.L.Sangeetha, M.Santhi, “Realtime Monitoring Of Cardiac Patients At Distance Using Tarang Communication”, International Journal of Innovative Research in Engineering & Science (IJIRES), Volume 9, Issue 3, September 2014, pp-15-20
- [18] G. Ofelt, Intensities of crystal spectra of rare-earth ions, J. Chem. Phys. 37, 511 (1962).
- [19] P.K Roy “Electromagnetic properties of Samarium sub Ni CU Zn ferrite prepared by auto combustion method” Journal of magnesium and magnetic material 247-251(2009).
- [20] S.K.A.Ahamed Kandu Sahib Magnetic Property Study of Nickel Cerium Doped Zinc Ferrite Nano Particles, International Journal of Computer Applications February 2012 (0975 – 8887) Volume 40– No.4.